Journal of Molecular Structure 1029 (2012) 60–67

Contents lists available at SciVerse ScienceDirect

Journal of Molecular Structure

journal homepage: www.elsevier.com/locate/molstruc

A new iron(III) complex of glycine derivative of amine-chloro substituted phenol ligand: Synthesis, characterization and catechol dioxygenase activity

Iraj Saberikia [a], Elham Safaei [a,*], Mohammad Hossein Kowsari [a], Yong-Ill Lee [b], Patricia Cotic [c], Giuseppe Bruno [d], Hadi Amiri Rudbari [d]

[a] Institute for Advanced Studies in Basic Sciences (IASBS), 45137-66731 Zanjan, Iran
[b] Department of Chemistry, Changwon National University, Changwon 641-773, South Korea
[c] Institute of Mathematics, Physics and Mechanics, University of Ljubljana, Ljubljana, Slovenia
[d] Dipartimento di Chimica Inorganica, Salita Sperone 31, Università di Messina, 98166 Messina, Italy

HIGHLIGHTS

- An iron(III) complex of glycine derivative of chloro-substituted bis(phenol)amine synthesized.
- The complex displayed paramagnetic and metal-centered reduction, and a ligand-centered oxidation.
- The oxygenation cleavage of catechol derivatives with this complex was investigated.

ARTICLE INFO

Article history:
Received 30 May 2012
Received in revised form 24 June 2012
Accepted 25 June 2012
Available online 4 July 2012

Keywords:
Amine bis(phenolate)
Non-heme iron
Model complex
Iron complex

ABSTRACT

A new iron(III) complex of the glycine derivative of amine-chloro substituted phenol ligand (H_3L^{GDC}) has been prepared and characterized by IR, ^{1}H NMR, UV–Vis spectroscopic techniques, cyclic voltammetry, ESI-MS and magnetic susceptibility studies. X-ray analysis reveals that in iron complex of FeL^{GDC} the iron(III) center has a distorted trigonal bipyramidal coordination sphere and is surrounded by an amine nitrogen, a carboxylate, a water and two phenolate oxygen atoms. The DFT calculations with the UB3LYP/6-311++G** level optimized structure of the complex are in good agreement with experimental X-ray structural data. The variable-temperature magnetic susceptibility indicates that FeL^{GDC} is the paramagnetic high spin iron(III) complex. It has been shown that electrochemical oxidation of this complex is ligand-centered due to the oxidation of phenolate to the phenoxyl radicals. This enzyme mimic utilized molecular oxygen in carrying out the oxidative cleavage of catechols with complete conversion at room temperature.

1. Introduction

Aromatic hydrocarbons are highly toxic environmental pollutants that can be degraded by bacteria under aerobic conditions. The aerobic biodegradation of these compounds is usually initiated by dioxygenases, which catalyze the oxidative cleavage of these compounds with concomitant insertion of both oxygen atoms of molecular oxygen into the aromatic ring of the substrate resulting in ring cleavage [1–3]. This large family of enzymes utilizes similar, mononuclear non-heme iron centers to activate the oxygen molecule to perform oxygenation at lateral positions and a variety of important biological functions [4–8]. Non-heme–iron dependent dioxygenase enzymes which catalyze the oxidative cleavage of catechol substrates are classified according to the different redox states of the iron associated with different reaction mechanisms [9]. The intradiol catechol dioxygenases utilize mononuclear iron(III) centers to catalyze the oxidative cleavage of the carbon–carbon bond between the two phenolic hydroxyl groups, while the extradiol-type enzymes contain a non-heme iron(III) molecule, cleave the adjacent carbon–carbon bond (Scheme 1).

Intradiol-type dioxygenases activate the metal-bound substrate, whereas the extradiol-type dioxygenases activate the O_2 bound to the iron, copper, manganese and magnesium containing dioxygenases have also been isolated [10].

Several bioinorganic modeling studies [9–30] have focused on the structural and spectroscopic characterization of iron(III) complexes of tripodal tetradentate, tetraaza macrocyclic and tetradentate bis(phenolate) ligands [12–14,19–31] as structural and functional models for the catecholate–iron(III) form of catechol dioxygenases. According to these studies, the significance of Lewis

* Corresponding author. Tel.: +98 241 4153200; fax: +98 241 4153232.
E-mail address: safaei@iasbs.ac.ir (E. Safaei).

0022-2860/$ - see front matter © 2012 Elsevier B.V. All rights reserved.
http://dx.doi.org/10.1016/j.molstruc.2012.06.047

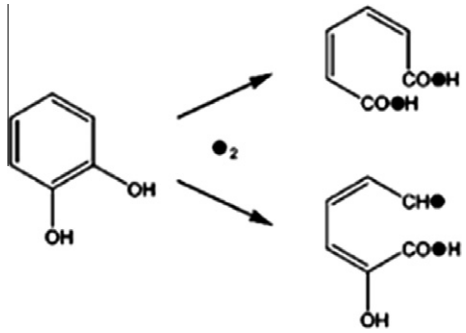

Scheme 1. Scheme of cleavage by intradiol and extradiol dioxygenases [7].

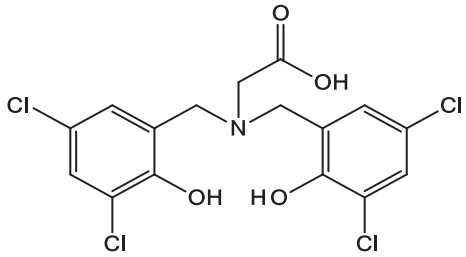

Scheme 2. Structure of [2-(bis(3,5-dichloro-2-hydroxybenzyl) amino) acetic acid] (H_3L^{GDC}).

acidity of iron(III) centers in the dioxygenase reactions have been highlighted [9–20].

In this paper, we report the synthesis, characterization, magnetic and redox properties, and catalytic activity of FeL^{GDC} complex of [N—O]-donor tripodal amine phenol ligand H_3L^{GDC}, 2-(bis-(3,5-dichloro-2-hydroxybenzyl)amino)acetic acid) (Scheme 2) which provide the coordination sphere around iron center. The oxygenation of catechol family with FeL^{GDC} as a functional model for catechol dioxygenases will be investigated with emphasize on the role of chlorine substituents on the catalytic activity of complex.

2. Experimental

2.1. Materials and physical measurements

Reagents or analytical grade materials were obtained from commercial suppliers and used without further purification, except those for electrochemical measurements. Elemental analyses (C, H, N) were performed by were performed by the Elementar, Vario EL III. Fourier transform infrared spectroscopy on KBr pellets was performed on a FT IR Bruker Vector 22 instrument. NMR measurements were performed on a Bruker 400 instrument. UV–Vis absorbance digitized spectra were collected using a CARY 100 spectrophotometer. The electronic spectra of the complex recorded in the CH_2Cl_2 solvent.

The ligand samples were dissolved in acetonitrile (1.0×10^{-4} M) and mixed with deionized water (1:1) just before the mass spectroscopic measurements. The identification of interaction products was performed using Thermo Finigan LCQ advantage ion trap mass spectrometer equipped with electrospray ionization. For sample injections, the instrument syringe pump was used at flow rate of 2 L/min. The instrumental operation conditions were as follows; spray voltage, 4.58 kV; source current, 0.48 A; sheath gas flow rate,19.43 L/min; capillary voltage; 9.44 V, capillary temperature 100 °C, tube lens voltage; 55 V. Experiments were performed in positive-ion mode and optimized by Xcalibur software before the experiments. All MS experiments in this work have been carried out under the optimized instrument conditions. All reported mass spectra are the average of at least 30 consecutive scans.

The mass spectrometry was performed on a QToF Premier (Waters, Manchester, UK) tandem mass spectrometer which had a quadrupole time-of-flight detector with orthogonal acceleration in V mode. The system was operated by MassLynx 4.1 software (Waters-Micromass, Manchester, UK) in positive ion electrospray mode. High purity nitrogen was used as the nebulizer and auxiliary gas, and argon was the collision gas. The nebulizer gas was set to 150 L/h at 150 °C and the cone gas and the source temperatures were set to 20 L/h and 90 °C, respectively. The capillary, extraction, and sample cone voltages were set to 3.0 V, 5.0 V, and 25 V, respectively. The instrument was operated in full-scan mode with QToF data collected between m/z 100–1000, with collision energy of 3 eV. The data were stored in the centroid mode with a scan time of 0.5 s and an inter scan delay of 0.01 s. The MS/MS experiments were performed using collision energies which were optimized for the corresponding analytes. Samples were injected at a flow rate of 5 μL/min. The QToF detector (MCP) was operated at 2100 V.

GC–MS was performed with a Clarus 600 GCMS (Perkin Elmer, Waltham, MA, USA). A 30 m capillary column coated with (5% diphenyl)dimethylpolysiloxane (0.25 mm i.d. and 1 μm film thichness; Elite-5MS, Perkin Elmer, Waltham, MA, USA) was used. The carrier gas was He at a flow 1.0 mL/min. Injection port and transfer line temperature was 270 °C. Samples were injected in methanol. The oven temperature program started at 70 °C (5 min), was raised at 20 °C/min to 200 °C, held for 15 min. and heated at 10 °C/min to 310 °C hold for 5.5 min. The quadrupole mass spectrometer was operated in EI mode (70 eV), scanning between m/z 40 and 520. The ion source temperature was 230 °C.

Magnetic susceptibility were measured from powder samples of solid material in the temperature range 2–300 K by using a SQUID susceptometer (Quantum Design MPMS-XL-5) in a magnetic field of 1000 Oe.

Voltammetric measurements were made with a computer controlled Auto Lab electrochemical system (ECO Chemie, Ultrecht, The Netherlands) equipped with a PGSTA 30 model and driven by GPES (ECO Chemie). A glassy carbon electrode with a surface area of 0.035 cm^2 was used as a working electrode and a platinum wire served as the counter electrode. The reference electrode was an Ag wire as the quasi reference electrode. Ferrocene was added as an internal standard after completion of a set of experiments, and potentials are referenced vs. the ferrocenium/ferrocene couple (Fc^+/Fc).

Diffraction data for FeL^{GDC} was measured on a Bruker–Nonius X8 ApexII diffractometer equipped with a CCD area detector by using graphite-monochromated Mo Kα radiation ($k = 0.71073$) generated from a sealed tube source. Data were collected and reduced by smart and saint software [32] in the Bruker package. The structure was solved by direct methods [33], than developed by least squares refinement on F^2 [34]. All non-H atoms were placed in calculated positions and refined as isotropic with the "riding-model technique". Details concerning collection and analysis are reported in Table 1.

2.2. Preparations

2.2.1. Synthesis of H_3L^{GDC}

The ligand was synthesized according to modified literature procedure [35–39]. As aqueous formaldehyde was one of the reagents, in some cases no added solvent was required beyond what was already present in the reagents solution.

A solution of 2,4-dichlorophenol (7.80 g, 48.00 mmol), 2-aminoacetic acid (1.8 g, 24.00 mmol), and 37% aqueous formaldehyde (3.58 mL, 48.00 mmol) was stirred and refluxed for 48 h. Upon cooling, a large quantity of beige solid was formed. The solvent

Table 1
Crystal data and structure refinement for $Fe_2(L^{THF})_3$.

Empirical formula	C32 H26 Cl8 Fe2 N4 O13
Formula weight	1069.87
Temperature (K)	296(2) K
Wavelength (Å)	0.71073 Å
Crystal system	Monoclinic
Space group	*I*2/*a*
a (Å)	*a* = 14.686(3) Å alpha = 90°
b (Å)	*b* = 8.8354(16) Å beta = 92.954(18)°
c (Å)	*c* = 33.720(8) Å gamma = 90°
Volume (Å^3)	4369.5(15) Å^3
Z	4
Calculated density (mg/m^3)	1.626 mg/m^3
Absorption coefficient (mm^{-1})	1.21–25.00°
F(000)	2152
Crystal size (mm)	0.41 × 0.14 × 0.02 mm
Theta range for data collection	1.21–25.00°
Limiting indices	$-17 \leqslant h \leqslant 17$, $-10 \leqslant k \leqslant 10$, $-40 \leqslant l \leqslant 40$
Reflections collected/unique	57648/3860 [*R*(int) = 0.1785]
Completeness	99.9%
Extinction coefficient	0.031(8)
Refinement method	Full-matrix least-squares on F^2
Data/restraints/parameters	3860/3/259
Goodness-of-fit on F^2	2.906
Final *R* indices [$I > 2\text{sigma}(I)$]	$R_1 = 0.2589$, $wR_2 = 0.6165$
R indices (all data)	$R_1 = 0.2938$, $wR_2 = 0.6476$
Largest diff. peak and hole (e A^{-3})	2.698 and −1.263 e A^{-3}

was decanted, and the remaining solid residue was washed with cold methanol to give a pure, white powder (6 g, 30% yield).

^{1}H NMR (400 MHz, DMSO, 298 K): δ 3.32 (s, 2H); 3.81 (s, 4H); 7.15 (d, 2H); 7.38 (d, 2H); 10.63 (br, $1H_{OH}$). ^{13}C NMR (400 MHz, DMSO, 298 K): δ 173.25, 151.60, 128.82, 128.52, 127.38, 123.18, 121.64, 54.42, 54.23.

^{13}C NMR (100.6 MHz, DMSO, 298 K): δ 173.2, 151.6, 128.8, 128.5, 127.3, 123.1, 121.6, 54.4, 54.2. IR (cm^{-1}): 3428 (OH); 3083 (OH); 2956 (C—H); 1733 (C=O); 1635 (C=C, phenyl ring). m.p. 207 °C.

2.2.2. Synthesis of FeL^{GDC}

Triethylamine (0.40 mL, 3.00 mmol) was added to a solution of H_3L^{GDC} (0.42 g, 1.00 mmol) in ethanol. $FeCl_3{\cdot}6H_2O$ (0.27 g, 1.00 mmol) was added to this solution and the resulting mixture was stirred for 1 h, resulting in an intense purple solution. The solvent was removed and the solid material recrystallized in 1:1 acetone/water mixture. Yield: 0.32 g (63%). Anal. calcd. for $C_{16}H_{10}Cl_5FeNO_4$ (510.84 g/mol): C, 37.21; H, 2.24; N, 3.00. Found: C, 37.42; H, 2.00; N, 2.68. IR (KBr, cm^{-1}): 3428, 3083, 2957, 1591, 1455, 1378, 1297, 1219, 1170, 1079, 1024, 924, 864, 810, 765, 575, 478. UV–Vis in CH_2Cl_2: λ_{max}, nm (ε, M^{-1} cm^{-1}): 289 (12800), 469 (2800). TOF-MSMS$_{([FeL^{GDC}]^+)}$: m/z = 518.9.

2.2.3. Spectrophotometric investigation of H_3L^{GDC} and Fe complexation

In an experiment, 2 mL of $Fe(NO_3)_3{\cdot}4H_2O$ solution in methanol (2.5×10^{-4} M) was transferred into a cuvette. UV–Vis spectra were recorded in the range of 300–800 nm about 5 min after each addition of 10 μL of H_3L^{GDC} (5×10^{-3} M) solution. Changes in the absorbance of iron nitrate complex upon addition of H_3L^{GDC} solution were monitored at the LMCT maximum wavelength of complexes.

2.2.4. Catalytic oxidation of 3,5-di-tert-butyl-catechol by FeL^{GDC}

FeL^{GDC} (with 5, 10, 50, 100 mmol percent) was added to a solution of triethylamine (2 mmol) in methanol 5 mL solvent (DMF, acetonitrile, ethanol and methanol) and (1 mmol) 3,5-di-*tert*-butyl-catechol (3,5-DTBC). The solution exposed to dioxygen and stirred for 48 h, the violet color slowly changed to dark green. The progress of the reaction was followed by TLC and ^{1}H NMR spectroscopy. Meanwhile both techniques showed the disappearance of 3,5-DTBC, the products were extracted from the aqueous solution with diethyl ether (3 × 30 mL). The organic layer was separated, washed with 2 M HCl (2 × 20 mL) and then dried over anhydrous Na_2SO_4 at room temperature and then filtered off and the filtrate was evaporated to give cleavage products in small amounts. The major product was quantified by comparing the TLC retention factor (R_f) values and ^{1}H NMR signals with the related values of the same sample reported previously [40].

The same experiment was repeated in the absence of any catalyst, no oxidation products were obtained. The complex (0.05 mmol), H_2DBC (0.222 g, 1.00 mmol), and Et_3N (280 mL, 2.0 mmol) were dissolved in 5 mL of one of solvent (DMF, acetonitrile, ethanol or methanol) and exposed to dioxygen and stirred for 48 h.

3. Results and discussion

This present ligand (2-(bis(3,5-dichloro-2-hydroxybenzyl) amino) acetic acid) H_3L^{GDC}) was synthesized according to known procedure [35–39] which involve employing methanol free Mannich condensation of the corresponding phenol, amine and formaldehyde. Since the formaldehyde used in the reaction contained 63% water, the process was carried in water instead of methanol as reported for similar aminophenol ligands. Iron complex FeL^{GDC} was easily formed in good yields by refluxing methanolic solution of the ligand with iron(III) chloride hexa-aqua and triethylamine in suitable ratio.

$$H_2L^{GDC} \xrightarrow[Ethanol,NEt_3]{FeCl_3.6H_2O} FeL^{GDC} \quad (1)$$

The strong band at around 3420–3440 cm^{-1}, corresponding to OH stretching mode of ligand, was replaced by a broad band in IR spectra of complex. This observation proves the coordination of phenol groups to the metal ion.

The electronic absorption spectra of FeL^{GDC} exhibit two bands in CH_2Cl_2 solution. The first band is apparent in 300–800 nm range (in the near UV), and one more in the visible region with high absorption coefficient (~12800 M^{-1} cm^{-1}). The lower energy band (460 nm) of FeL^{GDC} is assigned to a charge-transfer transition from the π orbital (HOMO) of the phenolate oxygen to the π* orbital of iron(III), and thus its band position falls in the range of other phenolato compounds (Section 2.2.2). The higher energy band (289 nm) is associated with the π orbital to π* orbital of the phenolate ion charge transfer (ILCT) [41–43].

Comparing the transition energies with ones for similar complex with amine-*tert*-butyl substituted phenol ligands [35] shows that both transitions shifted to higher energies. It can attributed to the electron-withdrawing effect of chlorine substituent on stabilizing phenolate π (HOMO) orbitals.

3.1. Spectral data analysis of H_3L^{GDC}–Fe complexation

The titrations of ligand (H_3L^{GDC}) solutions have been conducted at fixed concentration of iron and varying concentration of H_3L^{GDC}. The titration spectra of iron nitrate upon increasing addition of H_3L^{GDC} are shown in Fig. 1. During the titration, the hypochromicity was observed without any shift in λ_{max} band of 469 nm, which represents the existence of interaction between H_3L^{GDC} and the iron ion. The appearance of two isosbestic points in iron nitrate spectra clearly indicates the existence of simple equilibrium between H_3L^{GDC} and FeL^{GDC}. The complex composition of 1:1 was determined by plotting the absorption changes vs. ligand to metal mole ratio (n_L/n_{Fe}). Fig. 2 shows a mole ratio plot of iron nitrate upon increasing addition of H_3L^{GDC}. The observed spectral changes were used to determine the binding constants using SQUAD software. SQUAD program has been developed to enable the

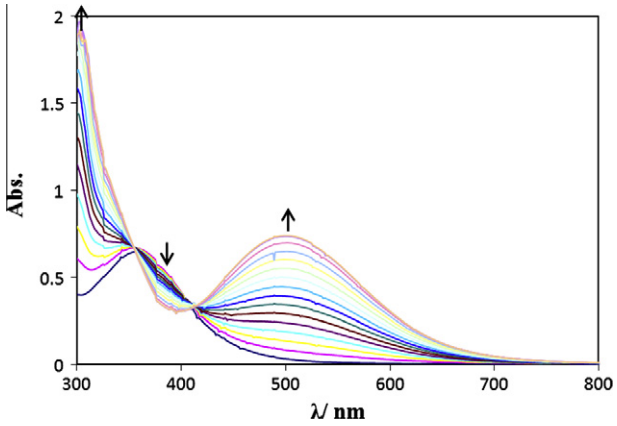

Fig. 1. The titration absorption spectra of $Fe(NO_3)_3{\cdot}4H_2O$ (2.5×10^{-4} M) by H_3L^{GDC}.

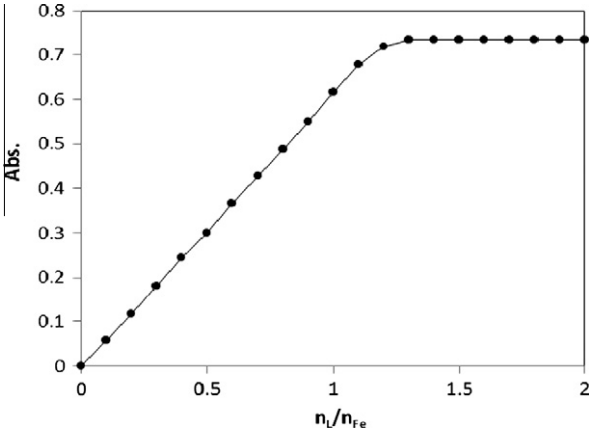

Fig. 2. Determination of FeL^{GDC} complex composition by the mole ratio plot.

evaluation of the best sets of binding constants from absorbance measurements by employing a non-linear least squares approach [44]. The input data consist of (a) the absorbance values and (b) the total H_3L^{GDC} and $Fe(NO_3)_3$ concentrations.

The Gauss–Newton non-linear least-squares algorithm is used for minimizing the residual sum of squares, U, which calculated from the the following equation:

$$U = \sum_{i=1}^{I}\sum_{k=1}^{NW}\left(A_{i,k}^{cal} - A_{i,k}^{obs}\right)^2 \quad (2)$$

where $A_{i,k}^{obs}$ is the absorbance value of ith solution at kth wavelength, give a total of I solutions and a grand total of NW wavelength. In our experiments I = 15 and NW = 50.

The output data are the logarithm of macroscopic formation constant (K_{ij}) for formation of FeL^{GDC} corresponding to the following equilibrium,

$$H_3L^{GDC} + Fe(NO_3)_3 \cdot 4H_2O \rightarrow FeL^{GDC} \quad (3)$$

The values of U and percent of error represent uncertainty for $\log K_{ij}$ calculated by the program.

The absorption data were analyzed by assuming 1:1 or 2:1 and/or simultaneous 1:1 and 2:1 M ratios of H_3L^{GDC} to $Fe(NO_3)_3$. Fitting of the experimental data (15 points), to the proposed stoichiometric models was evaluated by the sum of squares of the calculated points by the model. The results show that the best fitting corresponds to the 1:1 complex model. The value of pK_f has been obtained 3.36 ± 0.07 for FeL^{GDC} complex.

3.2. ESI-MS of FeL^{GDC}

The chemical compositions of complexes were established by TOF-MSMS spectrometry. The ESI-MS spectrum gave a prominent peak at m/z 500.89 $[(FeL^{GDC})]^+$, which clearly indicated the formation of 1:1 complex between Fe and H_3L^{GDC} and a water molecule correspondence to X-ray analysis and spectrophotometric titration method (Section 3.1). The ion peak with lower intensity appeared at m/z 518.9 is correspondence to FeL^{GDC} complex including Fe atom, H_3L^{GDC} and two water molecules. Furthermore, other peaks in the mass spectrum revealed the pattern that began with the loss of the carboxylic group (m/z 455.9) then a water molecule and CH_2 methylene group (m/z 414.8), followed by loss of three chlorine groups (m/z 316.9) after that iron and three oxygen atoms of phenolates (m/z 198.96), then a phenyl group (m/z 133.05). The mass spectrum of FeL^{GDC} is given in Fig. 3. It is worth noting that this ESI-MS, and consequently chemical composition is the same as that for the similar iron(III) complex with amine-bis(*tert*-butyl substituted phenolate), $L^{Gly}Fe$ [35]. The TOF-MS spectrum gave some $[L^{Gly}Fe]^+$ ion peak at m/z 587.00 (Fig. 1S) correspondence to the molecular weight of a 1:1 complex between Fe and H_3L^{Gly} including a water molecule. This difference (m/z $_{LGlyFe}$–m/z $_{FeLGDC}$) is exactly the difference between molecular weights of four *tert*-butyl and chlorine substituents. X-ray analysis of this complex has revealed that in $L^{Gly}Fe$, the iron(III) center is surrounded by the mentioned ligand while carboxylate group acts as bridging ligand for four coordinated iron centers of neighbor complexes leading to the formation of the infinite chains of the $L^{Gly}Fe$ units [35]. Based on similarities of ESI-MS of both complexes one can predict that FeL^{GDC} has the same structure as $L^{Gly}Fe$.

3.3. X-ray crystal structure of FeL^{GDC}

The diffraction experiment and the crystal data are summarized in Table 1. The selected bond lengths and angles are given in Table 2.

The asymmetric part of the reported structure is composed of a ferric center ligated by an H_3L^{GDC} ligand and a water molecule coordinated to the metal as shown in Fig. 4.

In the FeL^{GDC}, each Fe ion has a $FeNO_4$ coordination sphere which has a 5-coordinate deformed geometry. The iron center is surrounded by oxygen atoms O1, O2 of the phenolates and O3 of carboxylate. An amine nitrogen N(1) and one oxygen atom O(4 or 4′) of the coordinated water molecule occupy forth and fifth positions. The phenolate O1 and O2 form short bonds to the Fe(III), the distances being 1.913(15) and 1.922(16) Å, respectively. The carboxylate O3 participates in the Fe1—O3 bond of 2.03(2) Å, while the O(3′) atom forms the 2.08(4) Å bond to the Fe1 at another probability level. The distances of the water molecule oxygen O4 from Fe(III) is 1.94(2) Å while the other oxygen O(4′) distance being 2.00(3) Å.

The longest bond within the coordination sphere is formed by N1 atom, with the Fe—N distance of 2.209(18) Å. Bond lengths are consistent with iron complexes of aminophenol ligands [45,42,46–50]. The suggested structure is correspondence to the molecular mass.

3.4. Geometry optimization calculations of FeL^{GDC}

As seen in metal coordination sphere (Fig. 4), two equal probabilities exist for connecting the oxygen of carboxylate (O3, O3′) or water (O4, O4′) to the Fe ion in FeL^{GDC} complex. On the base of the X-ray data of this complex, density functional theory (DFT) calculations have been performed using Gaussian 09 suite of programs [51] for more insight into occupied atomic sites of the Fe coordination sphere. Two separate molecular structural optimizations in correspond with two mentioned probabilities around of metal

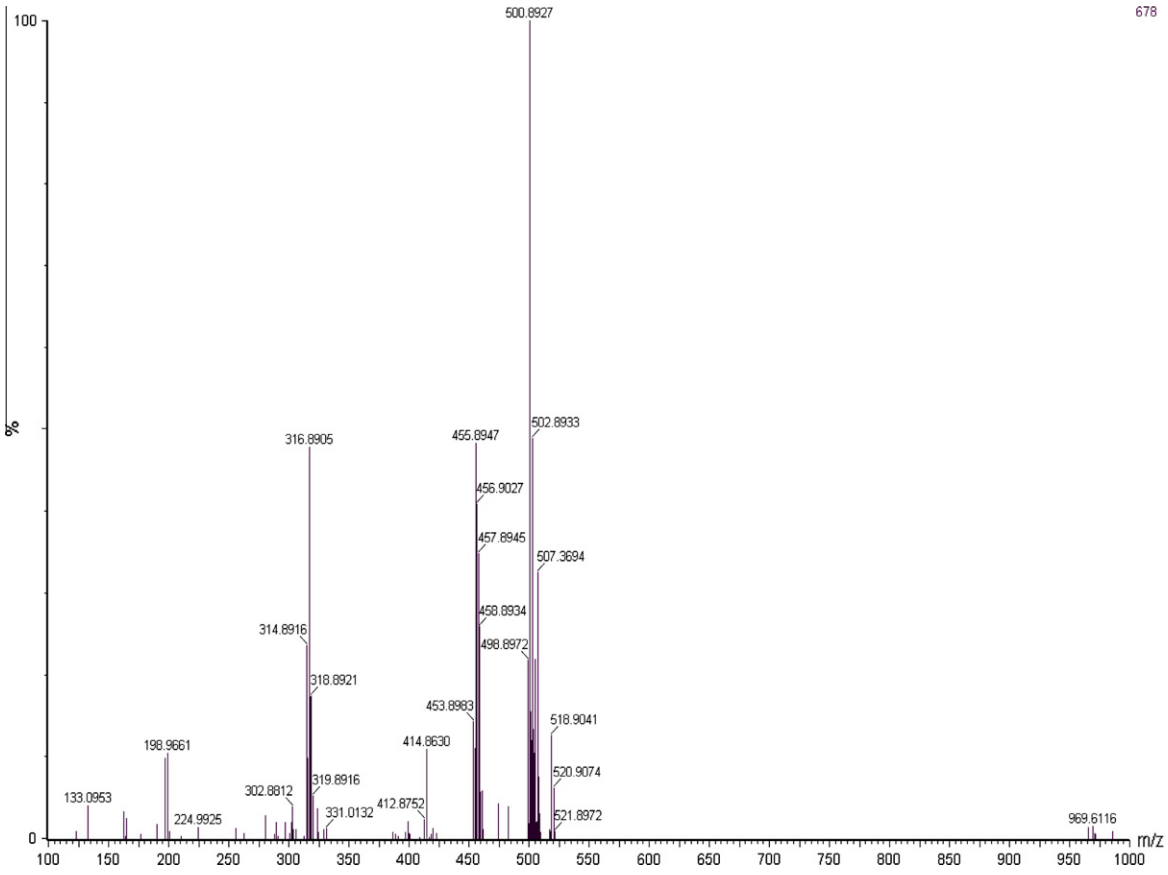

Fig. 3. ESI–MS spectrum of FeL^{GDC}.

Table 2
Selected bond lengths (Å) and angles (°) for $Fe_2(L^{THF})_3$.

O(4)—Fe	1.94(2)	O(4)—Fe—O(3)	41.8(13)
O(3)—Fe	2.03(2)	O(4′)—Fe—O(3)	95.0(13)
O(4′)—Fe	2.00(3)	O(2)—Fe—O(3′)	104.4(12)
O(3′)—Fe	2.08(4)	O(4)—Fe—O(3′)	91.3(7)
Fe—O(2)	1.922(16)	O(4′)—Fe—O(3′)	95.0(13)
Fe—O(1)	1.913(15)	O(3)—Fe—O(3′)	69.2(12)
Fe—N(1)	2.209(18)	O(1)—Fe—O(3′)	149.9(11)
O(2)—Fe—O(1)	97.2(7)	O(2)—Fe—N(1)	89.5(7)
O(2)—Fe—O(4)	82.1(9)	O(1)—Fe—N(1)	91.3(7)
O(1)—Fe—O(4)	165.5(10)	O(4)—Fe—N(1)	103.2(10)
O(2)—Fe—O(4′)	95.3(11)	O(4′)—Fe—N(1)	163.6(11)
O(1)—Fe—O(4′)	103.6(11)	O(3)—Fe—N(1)	85.2(8)
O(4)—Fe—O(4′)	62.2(12)	O(3′)—Fe—N(1)	68.6(10)
O(2)—Fe—O(3)	172.9(9)	O(4′)—Fe—O(3)	88.5(12)
O(1)—Fe—O(3)	87.6(8)	O(4)—Fe—O(3)	94.5(11)

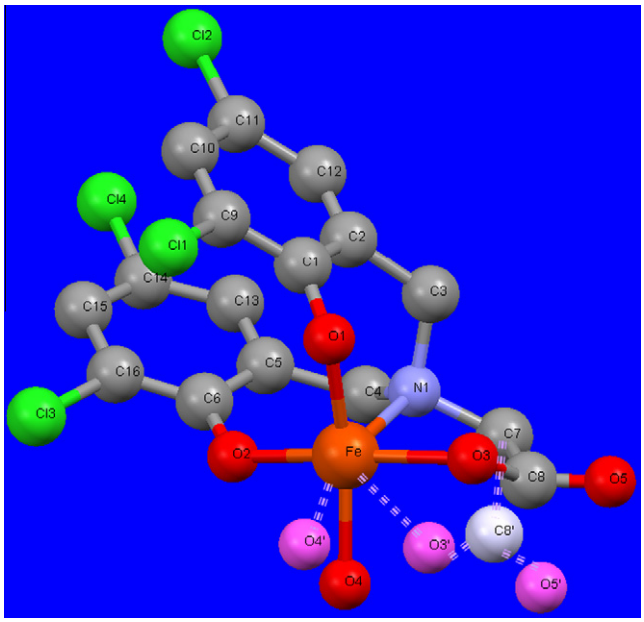

Fig. 4. ORTEP diagram and atom labeling scheme for the asymmetric unit of complex $L^{Gly}Fe$. Ellipsoids are plotted at 50 probability level. Hydrogen atoms omitted for clarity.

center have been carried out at the UB3LYP/6-311++G** level. In both initial molecular structures, the oxygen atom of water molecule (O4 or O4′) manually put at a distance of 2.5 Å from the Fe ion. Some of bond lengths and angles around Fe center in the optimized structures and their comparison with experimental X-ray values for current Fe complex are summarized in Table 3. Except of the expected differences originating from two types water definition (see i and ii in Table 3) in calculations and two placements of the O4 and O4′ groups around the Fe ion, the differences between other calculated bond lengths from the two calculations are negligible and we report a single calculated value for each of the bond length in Table 3. In general, the calculated bond lengths and angles are in good agreement with X-ray experiment. When 3-atomic sites of water were considered in calculation (i), the differences between corresponding calculated bond lengths, Water(O4)—Fe and Water(O4′)—Fe, with X-ray data are higher than that of other applied calculation using single oxygen site as indicator of water molecule (ii). In the next stage, to determine the

Table 3
Comparison of selected bond lengths (Å) and angles (°) of FeL^{GDC} complex from the molecular geometry optimizations by UB3LYP method using 6-311++G** basis set and experimental X-ray structure.

Bond	Bond length (calc.) (Å)	Bond length (X-ray) (Å)
Phenolate(O1)—Fe	1.866	1.913(15)
Phenolate(O2)—Fe	1.870	1.922(16)
Carboxylate(O3)—Fe	1.933	2.03(2)
Carboxylate(O3′)—Fe	1.930	2.08(4)
Water(O4)—Fe	2.164[a], 1.884[b]	1.94(2)
Water(O4′)—Fe	2.155[a], 1.884[b]	2.00(3)
N1—Fe	2.247	2.209(18)
O1—C1	1.338	1.33(2)
O2—C6	1.330	1.34(2)
O3—C8	1.315	1.55(5)
O3′—C8′	1.315	1.27(5)
N1—C3	1.501	1.48(3)
N1—C4	1.499	1.39(3)
N1—C7	1.491	1.48(3)
C1—C2	1.413	1.44(3)
C1—C9	1.406	1.43(3)
C6—C5	1.412	1.44(3)
C6—C16	1.407	1.36(3)
C8—C7	1.541	1.60(5)
C8—O5	1.209	1.189(19)
C8′—C7	1.541	1.44(4)
C8′—O5′	1.209	1.158(14)
Cl(1)—C9	1.748	1.68(2)
Cl(2)—C11	1.757	1.711(19)
Cl(3)—C16	1.750	1.72(2)
Cl(4)—C14	1.757	1.68(2)
Angle	**Bond angle (calc.) (°)**	**Bond angle, (X-ray) (°)**
O1—Fe—O2	114.34[a], 96.88[b]	97.2(7)
O1—Fe—N1	89.14[a], 81.47[b]	91.3(7)
O2—Fe—N1	91.41[a], 86.46[b]	89.5(7)
Fe—O1—C1	119.4[a], 129.61[b]	123.5(10)
Fe—O2—C6	129.56[a], 130.08[b]	129.7(12)
C3—N1—C4	113.14[a], 113.07[b]	107.7(19)
N1—C3—C2	116.49[a], 114.93[b]	117.2(2)
N1—C4—C5	116.25[a], 115.12[b]	120.2(18)

[a] The calculated bond length and angle when 3-atomic sites of water were considered in calculation).
[b] The calculated bond length and angle when the single oxygen site used as indicator of water molecule in calculation).

distortions of the real structure of the complex, all atomic sites from X-ray data are frozen except of hydrogen atoms of the complex and coordinated water molecule. We also determined the energy gap between HOMO and LUMO orbitals of FeL^{GDC} complex from the structure obtained in the calculations which are reported in Table 4.

3.5. Magnetic susceptibility measurements

Magnetic susceptibility for powdered samples of FeL^{GDC} was measured in a magnetic field of 1000 Oe as a function of temperature in the range 2–300 K. The measured data were corrected for

Table 4
The total energy (in Hartree) and the energy gap (in eV) between HOMO and LUMO orbitals of FeL^{GDC} complex calculated at the UB3LYP/6-311++G** level for two probabilities (normal and prim (′) coordinating conditions shown in Fig. 4). In runs 2 and 2′, all of non-hydrogen atomic sites of complex are frozen.

Run	Energy (a.u.)	HOMO–LUMO gap (eV)	
		α	β
Run-1 (full optimization)	−4152.8143834	0.17409	0.09743
Run-1′ (full optimization)	−4152.8142501	0.17398	0.09816
Run-2 (frozen non-H sites)	−4152.6577175	0.14159	0.07117
Run-2′ (frozen non-H sites)	−4152.7054438	0.15526	0.07106

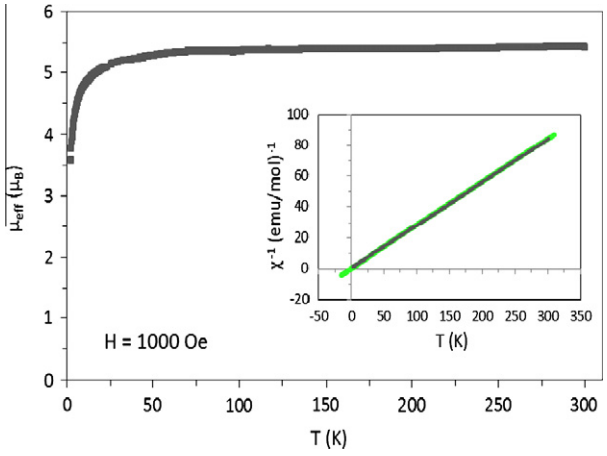

Fig. 5. Magnetic measurements for complex FeL^{GDC}.

the temperature-independent Larmor diamagnetic susceptibility obtained from the Pascal's tables [52,53] and for the sample holder contribution. The magnetic diagram is presented in Fig. 5 in the form of μ_{eff} vs. T and as inverse susceptibility vs. T (inset).

Above $T \approx 40$ K, the effective magnetic moment (μ_{eff}) of the complex FeL^{GDC} is essentially temperature-independent and has μ_{eff} value of 5.43 μ_B, which is close to the spin-only value of 5.92 μ_B for the isolated $S = 5/2$ Fe(III) ion. Thus the magnetic measurement of this complex shows unambiguously that FeL^{GDC} contains the magnetically diluted high-spin d^5 iron(III) ion.

Below 40 K, the effective magnetic moment (μ_{eff}) slightly decreases. Decrease of the effective magnetic moment might be due to a zero field splitting [52,53]. We applied a Curie–Weiss law $\chi = C/(T - \theta)$ to fit the high temperature data (above 100 K) which is shown as the inset in Fig. 5. The result (full line on the graph) almost passes the origin of the coordinate system showing the Curie–Weiss temperature to be near $\theta = 0.0$ K. This result led us to the conclusion that the contribution of zero field splitting in the effective magnetic moment declines at low temperature.

3.6. Electrochemistry

Cyclic and differential pulse voltammograms (CV and DPV) of the iron(III) complex were recorded in CH_2Cl_2 solutions containing

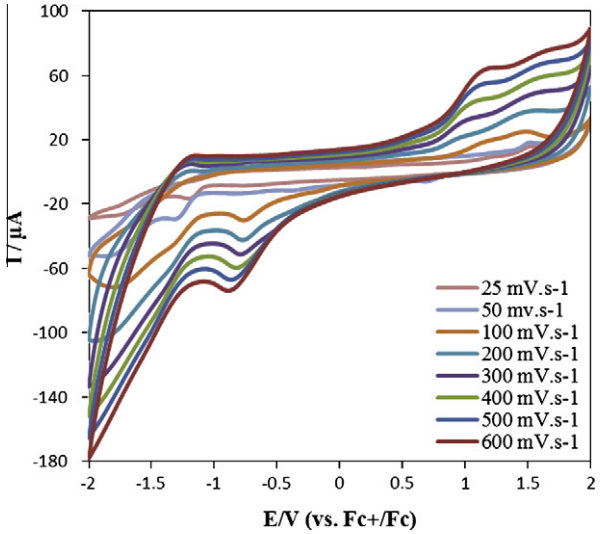

Fig. 6. Cyclic voltammograms of FeL^{GDC} (3×10^{-3} M) in CH_2Cl_2 with 0.1 M $[(nBu)_4N]ClO_4$ as supporting electrolyte. Potentials are referenced vs. Fc, scan rate is 50, 100, 200, 300, 400, 500 and 600 mV/s and $T = -40$ °C.

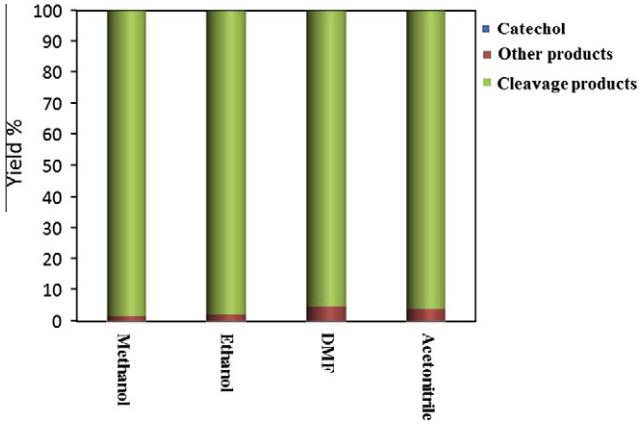

Fig. 7. Distribution of cleavage products catalyzed by FeL^{GDC} in different solvents (DMF, acetonitrile, ethanol and methanol).

0.1 M $[(nBu)_4N]ClO_4$ as supporting electrolyte. Prior to the measurement, the GC electrode was polished with 0.1 μm alumina powder and washed with distilled water. The voltage scan rate was set at 50 mV s^{-1}. The solutions were deoxygenated by bubbling nitrogen gas through them for 10 min. Ferrocene was added as an internal standard and potentials were referenced vs. the ferrocenium/ferrocene couple (Fc^+/Fc).

The CV voltammogram (CV) observed for this complex revealed oxidations and reductions peaks. In CH_2Cl_2 solution, this complex exhibits irreversible anodic redox behavior in the positive potential range assigned to the ligand-centered oxidation yielding the phenoxyl radical in the complex. The metal-centered voltammograms have been observed in the negative potential range corresponding with the Fe(III)/Fe(II) reduction of FeL^{GDC} (Fig. 6). The CV voltammograms with higher scan rates in low temperature show higher cathodic and anodic currents due to lowering chemical side reactions.

Comparing the reduction potential of iron center in this complex with the same *tert*-butyl substituted phenol-amine complex [35] shows a positive shift in FeL^{GDC} redox potential because of more highly positive charge density on iron center due to electron-withdrawing effects of chlorine substituent.

3.7. FeL^{GDC} catalyzed oxygenation of catechol family

The focus of this experimental part was to catalyze the oxygenation of catechols with different substituents with dioxygen as an oxidant. In the presence of 5% of the catalyst, 100% of 3,5-di-*tert*-butyl-catechol (3,5-DTBC) was converted to different cleavage products. This observation was in contrast to our previous results for the same reaction catalyzed by $L^{Gly}Fe$ [35] in which 3,5-DTBC was oxidized to produce 3,5-di-*tert*-butyl-*o*-benzoquinone (3,5-DTBQ) as the major product. This criterion is attributed to the higher Lewis acidity of metal center in FeL^{GDC} which facilitate oxidative cleavage of catechols. Our UV–Vis spectra and electrochemical results confirm this claim.

Progress of the reaction was followed by ^1H NMR spectroscopy. The signals of the free substrate (δ = 6.90, 1.37, 1.23) disappeared along with the appearance of another signals [44,45]. The reaction was monitored with different solvents (MeOH, EtOH, CH_3CN, DMF) and catalyst weight to choose methanol as the best solvent and 5% mmol of catalyst as proper loading of the catalyst. GC–MS technique was used to identify and quantify the oxidative products of 3,5-DTBC. The results are shown in Fig. 7.

The ^1H NMR and GC–mass show the 100% conversion of catechols and lacking any oxidized quinone product. Finally, the results show that FeL^{GDC} complex can act as a good catalyst for the oxygenation of catechol family to cleavage products in the presence of oxygen.

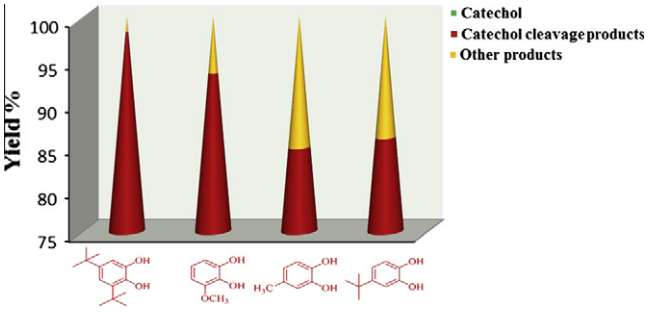

Fig. 8. Distribution of cleavage products catalyzed by FeL^{GDC} in methanol.

Table 5
Oxygenation cleavage products of catechol derivatives with FeL^{GDC} complex as a catalyst.

Substrate	Solvent	% Cleavage products	% Other products	% Conversion
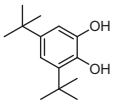	MeOH	98.21	1.79	100
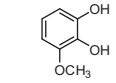	MeOH	93.40	6.60	100
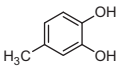	MeOH	84.80	15.20	100
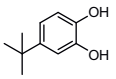	MeOH	85.94	14.06	100

The oxidative cleavage reaction of catechol derivatives with this complex was performed and the results are shown in Fig. 8 and Table 5.

4. Conclusion

The ligand [2-(bis(3,5-dichloro-2-hydroxybenzyl)amino)acetic acid], H_3L^{GDC} was prepared by a simple synthesis. The iron(III) complex of this tripodal tetradentate ligand was synthesized and characterized.

The chemical compositions of iron(III) complex were established by TOF-mass spectrometry and C, H, N analysis. Both techniques confirm 1:1 ratio of ligand to iron nitrate. The optimized structure of the complex from DFT calculation is in good agreement with experimental X-ray funding.

The variable temperature magnetic susceptibility indicates that FeL^{GDC} is the paramagnetic high spin iron(III) complex in almost the entire investigated temperature range. At low temperatures, the effective magnetic moment slightly decreases which is very probable due to the zero field splitting.

Redox process of $Fe^{III}L^{GDC}$ yielded the corresponding Fe(III)-phenoxyl radical and $Fe^{II}L^{GDC}$ species during the cyclic voltammetry experiments. A study of the phenolate-to-Fe(III) charge transfer band showed that substitution of a more electronegative substituent results in a red shift of the LMCT band and a positive shift of the Fe(III)/(II) redox potential. As a result, the phenolate-to-Fe(III) charge-transfer band indicates the redox potential of the iron

center concluding its ability for oxygenation. The catalytic experiments show that FeL^{GDC} complex acts as an excellent catalyst for cleavage oxygenation of catechols in the presence of oxygen. These observations will be helpful in designing proper ligands and modulation of the effective Lewis acidity and reactivity of the ferric center by the ligand.

Acknowledgments

Authors are grateful to the Institute for Advanced Studies in Basic Sciences (IASBS), Changwon, Ljubljana and Messina Universities for their valuable help. Special thanks to Dr. Saman Alavi for useful comments and manuscript editing. E. Safaei gratefully acknowledges the support by the Institute for Advanced Studies in Basic Sciences (IASBS) Research Council under Grant No. G2012IASBS127.

Appendix A. Supplementary material

The structural data for FeL^{GDC} has been deposited with the Cambridge Crystallographic Data Centre, the deposition number being CCDC 863642. This data can be obtained free of charge via http://www.ccdc.cam.ac.uk/conts/retrieving.html, or from the Cambridge Crystallographic Data Centre, 12 Union Road, Cambridge CB2 1EZ, UK; fax: +44 1223 336 033; or e-mail: deposit@ccdc.cam.ac.uk. Supplementary data associated with this article can be found, in the online version, at http://dx.doi.org/10.1016/j.molstruc.2012.06.047.

References

[1] E.Y. Tshuva, S.J. Lippard, Chem. Rev. 104 (2004) 987–1012.
[2] M. Costas, M.P. Mehn, M.P. Jensen, L. Que, Chem. Rev. 104 (2004) 939–986.
[3] J.D. Lipscomb, A.M. Orville, in: H. Sigel, A. Sigel (Eds.), Degradation of Environmental Pollutants by Microorganisms and their Metalloenzymes, Marcel Dekker, New York, 1992, pp. 243–298.
[4] L. Que, R.Y.N. Ho, Chem. Rev. 96 (1996) 2607–2624.
[5] E.I. Solomon, T. Brunold, M.I. Davis, J.N. Kemsley, S.K. Lee, N. Lehnert, F. Neese, A.J. Skulan, Y.S. Yang, Zhou, J. Chem. Rev. 100 (2000) 235–349.
[6] S. Dagley, in: J.R. Sokatch, L.N. Ornston (Eds.), Biochemistry of Aromatic Hydrocarbon Degradation in Pseudomonas, Academic Press, Orlando, 1986, pp. 527–555.
[7] M.A. Levin, M.A. Gealt, in: M.A. Levin, M.A. Gealt (Eds.), Biotreatment of Industrial and Hazardous Waste, McGraw-Hill, New York, 1993, pp. 5–7.
[8] T.D.H. Bugg, Tetrahedron 59 (2003) 7075–7101.
[9] D.D. Cox, L. Que, J. Am. Chem. Soc. 110 (1988) 8085–8092.
[10] F. Fusetti, K.H. Schroter, R.A. Steiner, P.I. van Noort, T. Pijning, H.J. Rozeboom, K.H. Kalk, M.R. Egmond, B.W. Dijkstra, Structure 10 (2002) 259–268.
[11] H.G. Jang, D.D. Cox, L. Que, J. Am. Chem. Soc. 113 (1991) 9200–9204.
[12] R.H. Heistand II, A.L. Roe, L. Que, Inorg. Chem. 21 (1982) 676–681.
[13] R.H. Heistand II, R.B. Lauffer, E. Fikrig, L. Que, J. Am. Chem. Soc. 104 (1982) 2789–2796.
[14] H. Fuji, Y. Funahashi, Angew. Chem., Int. Ed. 41 (2002) 3638–3641.
[15] T. Funabiki, T. Yamazaki, A. Fukui, T. Tanaka, S. Yoshida, Angew. Chem., Int. Ed. 37 (1998) 513–515.
[16] T. Funabiki, A. Mizoguchi, T. Sugimoto, S. Tada, M. Tsuji, H. Sakamoto, S. Yoshida, J. Am. Chem. Soc. 108 (1986) 2921–2932.
[17] R. Viswanathan, M. Palaniandavar, T. Balasubramanian, P.T. Muthiah, Inorg. Chem. 37 (1998) 2943–2951.
[18] M. Palaniandavar, R. Viswanathan, Chem. Sci. 108 (1996) 235–249.
[19] R. Viswanathan, M. Palaniandavar, T. Balasubramanian, P.T. Muthiah, J. Chem. Soc., Dalton Trans. (1996) 2519–2525.
[20] R. Viswanathan, M. Palaniandavar, J. Chem. Soc., Dalton Trans. (1995) 1259–1266.
[21] M. Pascaly, M. Duda, F. Scweppe, K. Zurlinden, F.K. Muller, B. Krebs, J. Chem. Soc., Dalton Trans. (2001) 828–837.
[22] P. Mialane, L. Tehertanov, F. Banse, J. Sainton, J.J. Girerd, Inorg. Chem. 39 (2000) 2440–2444.
[23] N. Raffard, R. Carina, A.J. Simaan, J. Sainton, E. Riviere, L. Tchertanov, S. Bourcier, G. Bouchoux, M. Delroisse, F. Banse, J.J. Girerd, Eur. J. Inorg. Chem. (2001) 2249–2254.
[24] W.O. Koch, V. Schünemann, M. Gerdan, A.X. Trautwein, H.J. Krüger, Chem. Eur. J. 4 (1998) 1255–1265.
[25] M. Velusamy, M. Palaniandavar, R. Srinivasagopalan, G.U. Kulkarni, Inorg. Chem. 42 (2003) 8283–8293.
[26] M. Velusamy, R. Mayilmurugan, M. Palaniandavar, Inorg. Chem. 43 (2004) 6284–6293.
[27] M. Palaniandavar, M. Velusamy, R. Mayilmurugan, J. Chem. Sci. 118 (2006) 601–610.
[28] M. Velusamy, R. Mayil Murugan, M. Palaniandavar, J. Inorg. Biochem. 99 (2005) 1032–1042.
[29] T. Dhanalakshmi, T. Bhuvanaeshwari, M. Palaniandavar, J. Inorg. Biochem. 100 (2006) 1527–1534.
[30] R. Mayilmurugan, M. Sankaralingam, E. Sureshb, M. Palaniandavar, Dalton Trans. 39 (2010) 9611–9625.
[31] Bruker AXS Inc., SMART, Version 5.060 and SAINT, Version 6.02, Wisconsin, USA, 1999.
[32] M.C. Burla, R. Caliandro, M. Camalli, B. Carrozzini, G.L. Cascarano, L. De Caro, C. Giacovazzo, G. Polidori, R. Spagna, J. Appl. Crystallogr. 38 (2005) 381–388.
[33] G.M. Sheldrick, SHELXL97, Program for Crystal Structure Refinement, University of Göttingen, Germany, 1997.
[34] SHELXT LN, Version 5.10, Bruker Analytical X-ray Inc., Madison, WI, USA, 1998.
[35] E. Safaei, H. Sheykhi, A. Wojtczak, Z. Jaglicic, A. Kozakiewicz, Polyhedron 30 (2011) 1143–1148.
[36] M.S. Shongwe, C.H. Kaschula, M.S. Adsetts, E.W. Ainscough, A.M. Brodie, M. Morris, J. Inorg. Chem. 44 (2005) 3070–3079.
[37] P. Amudha, M. Thirumavalavan, Polyhedron 18 (1999) 1371–1375.
[38] S. Groysman, I. Goldberg, M. Kol, E. Genizi, Z. Goldschmidt, Organometallics 23 (2004) 1880–1890.
[39] J.G. Wilson, Aust. J. Chem. 43 (1990) 1283–1289.
[40] V.I. Lodyato, I.L. Yurkova, V.L. Sorokin, O.I. Shadyro, V.I. Dolgopalets, M.A. Kisel, Bioorg. Med. Chem. Lett. 13 (2003) 1179–1182.
[41] M.I. Davies, A.M. Orville, F. Neese, J.M. Zaleski, J.D. Lipscomb, E.I. Solomon, J. Am. Chem. Soc. 124 (2002) 602–614.
[42] R. Mayilmurugan, E. Suresh, M. Palaniandavar, Inorg. Chem. 46 (2007) 6038–6049.
[43] R. Mayilmurugan, K. Visvaganesan, E. Suresh, M. Palaniandavar, Inorg. Chem. 48 (2009) 8771–8783.
[44] D.J. Leggett, W.A.E. McBryde, Anal. Chem. 47 (1975) 1065–1070.
[45] C. Imbert, H.P. Hratchian, M. Lanznaster, M.J. Heeg, L.M. Hryhorczuk, B.R. McGarvey, H.B. Schlegel, C.N. Verani, Inorg. Chem. 44 (2005) 7414–7422.
[46] M. Lanznaster, A. Neves, A.J. Bortoluzzi, B. Szpoganicz, E. Schwingel, Inorg. Chem. 41 (2002) 5641–5643.
[47] C.N. Verani, E. Bothe, D. Burdinski, T. Weyhermuller, U. Florke, P. Chaudhuri, Eur. J. Inorg. Chem. 8 (2001) 2161–2169.
[48] I.A. Setyawati, S.J. Rettig, C. Orvig, Can. J. Chem. 77 (1999) 2033–2038.
[49] J. Hwang, K. Govindaswamy, S.A. Koch, Chem. Commun. (1998) 1667–1668.
[50] D.M. Kurtz, Chem. Rev. 90 (1990) 585–606.
[51] M.J. Frisch, G.W. Trucks, H.B. Schlegel, G.E. Scuseria, M.A. Robb, J.R. Cheeseman, G. Scalmani, V. Barone, B. Mennucci, G.A. Petersson, H. Nakatsuji, M. Caricato, X. Li, H.P. Hratchian, A.F. Izmaylov, J. Bloino, G. Zheng, J.L. Sonnenberg, M. Hada, M. Ehara, K. Toyota, R. Fukuda, J. Hasegawa, M. Ishida, T. Nakajima, Y. Honda, O. Kitao, H. Nakai, T. Vreven, J.A. Montgomery, Jr., J.E. Peralta, F. Ogliaro, M. Bearpark, J.J. Heyd, E. Brothers, K. N. Kudin, V.N. Staroverov, R. Kobayashi, J. Normand, K. Raghavachari, A. Rendell, J.C. Burant, S.S. Iyengar, J. Tomasi, M. Cossi, N. Rega, J.M. Millam, M. Klene, J.E. Knox, J.B. Cross, V. Bakken, C. Adamo, J. Jaramillo, R. Gomperts, R. E. Stratmann, O. Yazyev, A.J. Austin, R. Cammi, C. Pomelli, J.W. Ochterski, R.L. Martin, K. Morokuma, V.G. Zakrzewski, G.A. Voth, P. Salvador, J.J. Dannenberg, S. Dapprich, A.D. Daniels, O. Farkas, J.B. Foresman, J.V. Ortiz, J. Cioslowski, D.J. Fox, Gaussian 09, Revision A.01, Gaussian, Inc., Wallingford CT, 2009.
[52] L. Dutta, A. Syamal, Elements of Magnetochemistry, Affiliated East-West Press Pvt. Ltd., New Delhi, 1993. pp. 6–11.
[53] C. Kittel, Introduction to Solid State Physics, eighth ed., John Wiley & Sons, New York, 2005 (Chapter 8).